The density-based many-body expansion as an efficient and accurate quantum-chemical fragmentation method: Application to water clusters

Daniel Schmitt-Monreal and Christoph R. Jacob*

Institute of Physical and Theoretical Chemistry, Technische Universität Braunschweig, Gaußstr. 17, 38106 Braunschweig, Germany

E-mail: c.jacob@tu-braunschweig.de

Abstract

Fragmentation methods based on the many-body expansion offer an attractive approach for the quantum-chemical treatment of large molecular systems, such as molecular clusters and crystals. Conventionally, the many-body expansion is performed for the total energy, but such an energy-based many-body expansion often suffers from a slow convergence with respect to the expansion order. For systems that show strong polarization effects such as water clusters, this can render the energy-based many-body expansion infeasible. Here, we establish a density-based many-body expansion as a promising alternative approach. By performing the many-body expansion for the electron density instead of the total energy and inserting the resulting total electron density into the total energy functional of density-functional theory, one can derive a density-based energy correction, which in principle accounts for all higher order polarization effects. Here, we systematically assess the accuracy of such a density-based many-body expansion for test sets of water clusters. We show that already a density-based two-body expansion is able to reproduce interaction energies per fragment within chemical accuracy, and is able to accurately predict the energetic ordering as well as the relative interaction energies of different isomers of water clusters.

Table of Contents Graphics

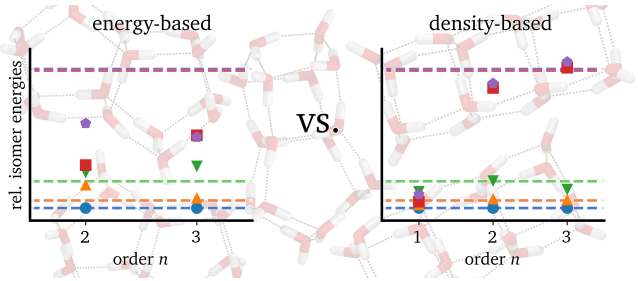

1 Introduction

Fragmentation methods offer an attractive approach for the quantum-chemical treatment of large molecular systems.[1–6] By replacing a single, full quantum-chemical calculation for the supermolecular system by many individual calculations for smaller fragments, the scaling of the computational effort with system size can be reduced, thus enabling the treatment of large systems that might be otherwise infeasible. Moreover, as the individual fragment calculations are in general independent of each other, these can be performed in a massively parallel fashion.[7–10] As they are naturally partitioned into their molecular building blocks, molecular clusters and molecular crystals present ideal use cases for the application of quantum-chemical fragmentation methods.[11–14] Water clusters provide a particularly interesting and intensely studied test case, as their interaction energies are determined by the hydrogen-bond network, in which considerable polarization and other cooperative effects can be present.[13,15–17]

The many-body expansion (MBE) probably constitutes the most straightforward fragmentation method.[18–23] In its simplest variant, the total energy of the full, supermolecular system is expanded as a sum of one-body, two-body etc. contributions,

$$E_{\text{tot}} = \sum_I E_I^{(1)} + \sum_{I<J} \Delta E_{IJ}^{(2)} + \sum_{I<J<K} \Delta E_{IJK}^{(3)} + \cdots \tag{1}$$

which are obtained from calculations for the isolated monomers, dimers, trimers, etc. Here, $E_I^{(1)}$ is the total energy of the I-th monomer, $\Delta E_{IJ}^{(2)}$ is the dimer interaction energy of the I-th and J-th monomer, $\Delta E_{IJK}^{(3)}$ is the trimer interaction energy of the I-th, J-th, and K-th monomer, and so on (see below for details). As only total energies of the fragments enter in Eq. (1), any quantum-chemical method can be directly used within such an *energy-based MBE* (eb-MBE).

While the MBE is by construction exact if all n-body contributions up to the total number of fragments N are included, it only offers a computational advantage if it can

be truncated at low order. If all contributions up to order n are included, the number of quantum-chemical fragment calculations scales as $\mathcal{O}(N^n)$. This scaling can be reduced by a suitable screening of higher-order contributions, for which various strategies have been developed.[23–26] For water clusters of increasing size, Herbert and coworkers found that in the eb-MBE the inclusion of three-body and four-body contributions is mandatory in order to obtain chemical accuracy in the total interaction energies.[23,27,28] However, the computational effort for the inclusion of four-body and higher-order contributions (and possibly already of the three-body contributions) is generally prohibitive.

Several strategies for accelerating the convergence of the MBE have been developed (see Ref. 29 for a recent review). First, the MBE can be combined with embedding methods (embedded MBE)[24,30,31] that account for the effect of the environment in each of the fragment calculations. Most common is the use of suitable point-charge embedding schemes,[32] but recently the use of more sophisticated quantum embedding schemes has also been explored.[33,34] Second, multilevel composite methods can be constructed based on the MBE, in which a cheaper low-level method (e.g., a polarizable force field) is used to calculate the higher-order many-body contributions that are otherwise neglected in a truncated MBE.[11,35–37] Third, the MBE can be generalized to overlapping fragments[38–40] and numerous fragmentation methods have been developed following this strategy.[41–46]

Recently, we have proposed *a density-based MBE* (db-MBE),[34] motivated by the observation that an MBE of the electron density,

$$\rho_{\text{tot}} = \sum_I \rho_I^{(1)} + \sum_{I<J} \Delta\rho_{IJ}^{(2)} + \sum_{I<J<K} \Delta\rho_{IJK}^{(3)} + \cdots \tag{2}$$

converges significantly faster than the conventional MBE of the total energy [cf. Eq. (1)]. In Eq. (2), the monomer (one-body) electron densities $\rho_I^{(1)}$ as well as the two-body, three-body, and higher-order difference densities $\Delta\rho_{IJ}^{(2)}$, $\Delta\rho_{IJK}^{(3)}$, and so on, are defined analogously to the corresponding energy terms. By inserting the MBE of the electron density into

the total energy functional of density-functional theory (DFT) and using explicit density functionals for all nonadditive energy terms in the spirit of subsystem DFT,[47–50] one can derive a density-based correction to the energy-based MBE that accounts for higher-order energy contributions. This density-based MBE formalism can be consistently combined with different embedding schemes for the fragment calculations.

Ideally, the truncation error of any MBE scheme should be below chemical accuracy already for a two-body approximation (pairwise additive approximation), which is rarely achieved if an energy-based MBE is employed,[29] even in combination with sophisticated embedding schemes.[33] Previously,[34] we successfully applied the density-based MBE to selected clusters of water and aspirin extracted from the respective crystal structures, but did not systematically assess its accuracy. Here, we set out to close this gap by thoroughly benchmarking the density-based MBE using water clusters as a challenging test case. We consider both the error in the total interaction energies for clusters of increasing size (see Sect. 3) and the error in relative interaction energies of different isomers of clusters of a given size (see Sect. 4).

2 Computational Methodology

2.1 Energy-Based Many-Body Expansion

The conventional, energy-based many-body expansion (eb-MBE)[22,29] decomposes the total energy of a system consisting of N molecular fragments as [cf. Eq. (1)],

$$E_{\text{tot}} = E^{(1)} + \Delta E^{(2)} + \Delta E^{(3)} + \cdots = E^{(1)} + \sum_{i=2}^{N} \Delta E^{(i)}. \tag{3}$$

Here, $E^{(1)} = \sum_I E_I^{(1)}$ are the one-body contributions obtained from calculations of the total energies $E_I^{(1)} = E_I$ of the N individual monomer, $\Delta E^{(2)} = \sum_{I<J} \Delta E_{IJ}^{(2)}$ are the two-body

contribution obtained from calculations of the interaction energies

$$\Delta E_{IJ}^{(2)} = E_{IJ} - E_I - E_J, \tag{4}$$

of the $N(N-1)/2$ possible dimers, where E_{IJ} is the total energy of the dimer consisting of the I-th and the J-th molecular fragment, and $\Delta E^{(3)} = \sum_{I<J<K} \Delta E_{IJK}^{(3)}$ are the three-body contributions obtained from the trimer interaction energies

$$\Delta E_{IJK}^{(3)} = E_{IJK} - \Delta E_{IJ}^{(2)} - \Delta E_{IK}^{(2)} - \Delta E_{JK}^{(2)} - E_I - E_J - E_K, \tag{5}$$

where E_{IJK} is the total energy of the trimer consisting of the I-th, J-th, and K-th molecular fragment. Higher-order interaction energies can be defined analogously, and general definitions can be found in, e.g., Ref. 51.

A computational advantage compared to a supermolecular calculation for the full system is only gained if the eb-MBE can be truncated at a sufficiently low order $n \ll N$, i.e.,

$$E_{\text{tot}} \approx E_{\text{eb-MBE}}^{(n)} = E^{(1)} + \sum_{i=2}^{n} \Delta E^{(i)}. \tag{6}$$

Such a truncation will introduce an error compared to a full, supermolecular treatment, but ideally, this error is sufficiently small already at a low expansion order. For many applications to molecular clusters, an accurate two-body expansion — with a computational effort increasing as $\mathcal{O}(N^2)$ — would be highly desirable.

In the simplest case, the individual single-point calculations for monomers, dimers, trimers, etc. are performed for the respective isolated systems, i.e., the remaining molecular fragments are completely neglected. We will refer to this variant of the MBE as *isolated MBE*. A commonly used strategy for accelerating the convergence of the MBE is the (approximate) inclusion of this environment into the calculations for the monomer, dimer, trimers, etc.[24,30–32] For the subsystem composed of the molecular fragments $\{I, J, \dots\}$, the effect of

this environment is included as a (local) embedding potential, $v_{\text{emb}}^{(IJ\cdots)}(\boldsymbol{r})$, which is due to the remaining molecular fragments $K \notin \{I, J, \dots\}$.

Here, we employ two variants of such an *embedded MBE*. First, we use an electrostatic point-charge embedding with the embedding potential commonly used in QM/MM approaches,

$$v_{\text{emb,PC}}^{(IJ\cdots)}(\boldsymbol{r}) = \sum_{K\notin\{I,J,\dots\}} \sum_{k\in K} \frac{q_k}{|\boldsymbol{r} - \boldsymbol{R}_k|}, \tag{7}$$

where q_k are suitable partial charges placed at the positions of the nuclei $\boldsymbol{R}_k$. Second, we consider the embedding potential of frozen-density embedding (FDE) theory,[50,52]

$$\begin{aligned} v_{\text{emb,FDE}}^{(IJ\cdots)}(\boldsymbol{r}) = & \sum_{K\notin\{I,J,\dots\}} v_{\text{nuc}}^{(K)}(\boldsymbol{r}) + \sum_{K\notin\{I,J,\dots\}} \int \frac{\rho_K(\boldsymbol{r}')}{|\boldsymbol{r} - \boldsymbol{r}'|}\,\mathrm{d}^3 r' \\ & + \left.\frac{\delta T_s[\rho]}{\delta\rho}\right|_{\rho=\rho_{\text{tot}}} - \left.\frac{\delta T_s[\rho]}{\delta\rho}\right|_{\rho=\rho_{IJ\cdots}} + \left.\frac{\delta E_{\text{xc}}[\rho]}{\delta\rho}\right|_{\rho=\rho_{\text{tot}}} - \left.\frac{\delta E_{\text{xc}}[\rho]}{\delta\rho}\right|_{\rho=\rho_{IJ\cdots}} \end{aligned} \tag{8}$$

with $\rho_{\text{tot}} = \rho_{IJ\cdots} + \sum_{K\notin\{I,J,\dots\}} \rho_K$. This embedding potential depends on the electron densities $\rho_K(\boldsymbol{r})$ of the monomers constituting the environment, which are obtained from calculations for the isolated monomers in the present study. It includes the full nuclear potentials $v_{\text{nuc}}^{(K)}(\boldsymbol{r})$ of the monomers in the environment as well as their full Coulomb potential. In addition, it also contains non-classical contributions due to the exchange–correlation and kinetic energy, which are evaluated using an approximate exchange-correlation (xc) functional $E_{\text{xc}}[\rho]$ and an approximate kinetic energy functional $T_s[\rho]$.

It is important to note that when using an embedded MBE, the total energies of the monomers, dimers, trimers, etc. that appear in Eq. (3) refer only to the active (embedded) subsystem and must exclude the interaction of this active subsystem with the embedding potential to avoid double-counting of interactions (see Ref. 34 for a detailed discussion).

2.2 Density-Based Many-Body Expansion

Starting point for the density-based MBE (db-MBE)[34] is a many-body expansion of the electron density [cf. Eq. (2)],

$$\rho_{\text{tot}}(\boldsymbol{r}) = \rho^{(1)}_{\text{tot}}(\boldsymbol{r}) + \Delta\rho^{(2)}_{\text{tot}}(\boldsymbol{r}) + \Delta\rho^{(3)}_{\text{tot}}(\boldsymbol{r}) + \cdots = \rho^{(1)}_{\text{tot}}(\boldsymbol{r}) + \sum_{i=1}^{N} \Delta\rho^{(i)}_{\text{tot}}(\boldsymbol{r}), \tag{9}$$

which can be truncated at order n,

$$\rho_{\text{tot}}(\boldsymbol{r}) \approx \rho^{(n)}_{\text{tot}}(\boldsymbol{r}) = \rho^{(1)}_{\text{tot}}(\boldsymbol{r}) + \sum_{i=1}^{N} \Delta\rho^{(i)}_{\text{tot}}(\boldsymbol{r}). \tag{10}$$

Here, $\rho^{(1)}_{\text{tot}}(\boldsymbol{r}) = \sum_I \rho^{(1)}_I$ is the sum of the monomer densities and $\Delta\rho^{(2)}_{\text{tot}}(\boldsymbol{r}) = \sum_{I<J} \Delta\rho^{(2)}_{IJ}$ is the sum of the dimer density corrections,

$$\rho^{(2)}_{IJ} = \Delta\rho^{(2)}_{IJ} = \rho_{IJ} - \rho^{(1)}_I - \rho^{(1)}_J, \tag{11}$$

where ρ_{IJ} is the electron density calculated for the dimer of the I-th and J-th fragment. The three-body and higher-order contributions are defined analogously to the corresponding energy corrections. As discussed for the eb-MBE above, an MBE of the electron density can either be performed as an isolated MBE or as an embedded MBE. Previously,[34] we noticed that such a MBE of the electron density usually converges faster than the conventional MBE of the total energy, in particular if a suitable embedding scheme is employed.

Within the framework of density-functional theory (DFT), the above (truncated) MBE of the electron density can then be used to obtain an approximation of the total energy as[34]

$$E_{\text{tot}} \approx E^{(n)}_{\text{db-MBE}} = E_{\text{tot}}\left[\rho^{(n)}_{\text{tot}}(\boldsymbol{r})\right], \tag{12}$$

where

$$E_{\text{tot}}[\rho] = T_s[\rho] + V_{\text{nuc}}[\rho] + J[\rho] + E_{\text{xc}}[\rho] + E_{\text{NN}} \tag{13}$$

is the well known total energy functional of Kohn–Sham DFT. Here, $T_s[\rho]$ is the noninteracting kinetic energy functional, which is commonly evaluated with the help of the KS orbitals $\{\phi_i\}$, $V_{\text{nuc}}[\rho] = \int \rho(\boldsymbol{r}) v_{\text{nuc}}(\boldsymbol{r})\, \mathrm{d}^3 r$ is the electron–nuclei attraction energy, $J[\rho] = \frac{1}{2} \iint \frac{\rho(\boldsymbol{r})\rho(\boldsymbol{r}')}{|\boldsymbol{r}-\boldsymbol{r}'|}\, \mathrm{d}^3 r \mathrm{d}^3 r'$ is the Coulomb energy, $E_{\text{xc}}[\rho]$ is the exchange–correlation (xc) functional, and E_{NN} is the nuclear repulsion energy.

Eq. (12) can be re-expressed as

$$E^{(n)}_{\text{db-MBE}} = E^{(n)}_{\text{eb-MBE}} + \left(E_{\text{tot}}\left[\rho^{(n)}_{\text{tot}}(\boldsymbol{r})\right] - E^{(n)}_{\text{eb-MBE}} \right) = E^{(n)}_{\text{eb-MBE}} + E^{(n)}_{\text{db-corr}}, \tag{14}$$

where $E^{(n)}_{\text{eb-MBE}}$ is the total energy obtained in a conventional, energy-based n-body expansion and $E^{(n)}_{\text{db-corr}}$ is a density-based interaction energy correction term. The first term can be evaluated in the conventional way using any quantum-chemical method — either based on DFT or wave-function theory — whereas the second term can be evaluated using approximate kinetic-energy and xc density functionals in the spirit of subsystem DFT.[50] Thus, the db-MBE can be viewed as an ONIOM-style[53,54] composite scheme in which orbital-free DFT is used as the low-level method.

At first order (i.e., for a one-body expansion using only monomer calculations), one obtains the density-based energy correction,

$$\begin{aligned} E^{(1)}_{\text{db-corr}} &= E_{\text{tot}}\left[\textstyle\sum_I \rho^{(1)}_I\right] - \textstyle\sum_I E_I \\ &= \sum_{I\neq J} \int \rho^{(1)}_I(\boldsymbol{r}) v^{(J)}_{\text{nuc}}(\boldsymbol{r})\, \mathrm{d}^3 r + \sum_{I<J} \iint \frac{\rho^{(1)}_I(\boldsymbol{r})\rho^{(1)}_J(\boldsymbol{r}')}{|\boldsymbol{r}-\boldsymbol{r}'|}\, \mathrm{d}^3 r \mathrm{d}^3 r' + \sum_{I<J} E^{(IJ)}_{\text{NN}} \\ &\quad + E^{\text{nadd}}_{\text{xc}}\left[\{\rho^{(1)}_I\}\right] + T^{\text{nadd}}_s\left[\{\rho^{(1)}_I\}\right] \end{aligned} \tag{15}$$

where $v^{(J)}_{\text{nuc}}(\boldsymbol{r}) = \sum_{j\in J} \frac{Z_j}{|\boldsymbol{r}-\boldsymbol{R}_j|}$ is the nuclear potential of the J-the molecular fragment and $E^{(IJ)}_{\text{NN}} = \sum_{i\in I}\sum_{j\in J} \frac{Z_i Z_j}{|\boldsymbol{R}_i-\boldsymbol{R}_j|}$ is the repulsion energy between the nuclei in the I-th and the

J-th fragment. The nonadditive kinetic-energy and xc energy functionals are defined as

$$T_s^{\text{nadd}}\Big[\{\rho_I^{(1)}\}\Big] = T_s\Big[\sum_I \rho_I^{(1)}\Big] - \sum_I T_s\Big[\rho_I^{(1)}\Big] \tag{16}$$

$$E_{\text{xc}}^{\text{nadd}}\big[\{\rho_I^{(1)}\}\big] = E_{\text{xc}}\Big[\sum_I \rho_I^{(1)}\Big] - \sum_I E_{\text{xc}}\Big[\rho_I^{(1)}\Big]. \tag{17}$$

These nonadditive functionals need to be evaluated using suitable approximate density functionals.[50,55,56] If the underlying eb-MBE is performed using DFT with an xc functional depending only on the electron density, such as a generalized-gradient approximation (GGA) functional, the nonadditive xc contribution can be evaluated consistently using the same approximate functional. If orbital-dependent xc functionals, such as hybrid or meta-GGA functionals, are employed or if a wavefunction-based quantum-chemical method is used, the nonadditive xc contribution has to be approximated using a GGA xc functional. In any case, an approximate kinetic-energy density functional has to be used to evaluate the nonadditive kinetic-energy contribution. The above first-order density-based energy correction is equivalent to the interaction energy expression used in subsystem DFT,[50,57] and when using electron densities $\rho_I^{(1)}$ obtained from calculations for the isolated fragments, corresponds to the Harris functional.[47,48]

When going to higher orders ($n \geq 2$), the density-based energy correction is given by,[34]

$$\begin{aligned} E_{\text{db-corr}}^{(n)} &= E_{\text{tot}}\Big[\rho_{\text{tot}}^{(n)}(\boldsymbol{r})\Big] - E_{\text{eb-MBE}}^{(n)} \\ &= \Big(V_{\text{nuc}}\Big[\rho_{\text{tot}}^{(n)}\Big] - V_{\text{nuc}}^{(n)}\Big) + \Big(J\Big[\rho_{\text{tot}}^{(n)}\Big] - J^{(n)}\Big) \\ &\quad + T_s^{\text{nadd},(n)}\Big[\{\rho_I\},\{\rho_{IJ}\},\dots\Big] + E_{\text{xc}}^{\text{nadd},(n)}\Big[\{\rho_I\},\{\rho_{IJ}\},\dots\Big] \end{aligned} \tag{18}$$

Here, the n-body nonadditive kinetic and xc energy functionals are defined as

$$T_s^{\text{nadd},(n)}\big[\{\rho_I\},\{\rho_{IJ}\},\dots\big] = T_s\big[\rho_{\text{tot}}^{(n)}\big] - T_s^{(n)} \tag{19}$$

$$E_{\text{xc}}^{\text{nadd},(n)}\big[\{\rho_I\},\{\rho_{IJ}\},\dots\big] = E_{\text{xc}}\big[\rho_{\text{tot}}^{(n)}\big] - E_{\text{xc}}^{(n)}, \tag{20}$$

when can be evaluated using suitable approximate density functionals. In the above equations, $T_s^{(n)}$ and $E_{\rm xc}^{(n)}$ are the truncated many-body expansions of the kinetic and xc energies (evaluated using suitable approximate functionals), respectively, and $V_{\rm nuc}^{(n)}$ and $J^{(n)}$ are the truncated n-body expansions of the electron-nuclei attraction and the electronic Coulomb energies, respectively, which are defined in analogy to corresponding expansions of the total energy defined in Eq. (6). The electron-nuclei attraction energy and the Coulomb energy of the many-body expanded electron density at n-th order, $\rho_{\rm tot}^{(n)}(\boldsymbol{r})$, can be evaluated recursively as,

$$V_{\rm nuc}\big[\rho_{\rm tot}^{(n)}\big] = V_{\rm nuc}\big[\rho_{\rm tot}^{(n-1)} + \Delta\rho_{\rm tot}^{(n)}\big] = V_{\rm nuc}\big[\rho_{\rm tot}^{(n-1)}\big] + \int \Delta\rho_{\rm tot}^{(n)}\, v_{\rm nuc}(\boldsymbol{r})\, {\rm d}^3r, \tag{21}$$

and,

$$\begin{aligned} J\big[\rho_{\rm tot}^{(n)}\big] &= J\big[\rho_{\rm tot}^{(n-1)} + \Delta\rho_{\rm tot}^{(n)}\big] \\ &= J\big[\rho_{\rm tot}^{(n-1)}\big] + \iint \frac{\rho_{\rm tot}^{(n-1)}(\boldsymbol{r})\Delta\rho_{\rm tot}^{(n)}(\boldsymbol{r}')}{|\boldsymbol{r}-\boldsymbol{r}'|}\, {\rm d}^3r{\rm d}^3r' + \frac{1}{2}\iint \frac{\Delta\rho_{\rm tot}^{(n)}(\boldsymbol{r})\Delta\rho_{\rm tot}^{(n)}(\boldsymbol{r}')}{|\boldsymbol{r}-\boldsymbol{r}'|}\, {\rm d}^3r{\rm d}^3r'. \end{aligned} \tag{22}$$

Note that the evaluation of $E_{\text{db-corr}}^{(n)}$ only requires the knowledge of the electron densities of the monomers, dimers, trimers etc. and is thus completely independent of the details of the quantum-chemical calculations employed in the underlying eb-MBE.

2.3 Computational Details

All quantum-chemical calculations have been performed using DFT as implemented in the Amsterdam Density-Functional (ADF) program package[58,59] in combination with the PyADF scripting framework.[60] The BP86[61,62] and B3LYP[63–65] xc functionals and a double-zeta plus polarization (DZP) basis set of Slater-type orbitals[66] as well as a Becke integration grid of "very good" accuracy[67] have been used throughout. All total energies have been obtained with ADF's total energy implementation.[68]

For the point-charge embedded MBEs we used TIP3P[69] point-charges ($q_{\mathrm{H}} = +0.417$ and $q_{\mathrm{O}} = -0.834$) for the environment water molecules. The frozen-density embedded MBE calculations made use of ADF's implementation of FDE[70] with the PW91k nonadditive kinetic-energy functional.[71] For the BP86 calculations, the same xc functional was used for the nonadditive xc contributions, whereas for the B3LYP calculations, the BLYP xc functional was chosen for these terms. In these FDE calculations, ADF's default integration grid as described in Ref. 72 has been employed.

The density-based energy correction of arbitrary order can be obtained with PyADF and its PyEmbed module, which provides a stand-alone implementation of the subsystem DFT embedding potential and interaction energy terms. The n-body nonadditive xc and kinetic energy [see Eqs. (19) and (20)] have been evaluated using the XCFun library[73,74] with the approximate functional specified above. The electrostatic interaction energies are calculated in PyEmbed by numerical integration from the electron densities and the nuclear and Coulomb potentials exported from ADF according to Eqs. (15), (21), and (22). Here, we used the supermolecular integration grid for the evaluation of all contributions to the density-based energy correction. Further details on the implementation are given in Ref. 34.

The most recent release version of PyADF, which contains our implementation of the density-based many-body expansion and which can be used in combination with the ADF program package to reproduce all calculations included in the present manuscript, is available at Ref. 75.

Cartesian coordinates of all molecular clusters used as test cases in this work are included as Supporting Information.

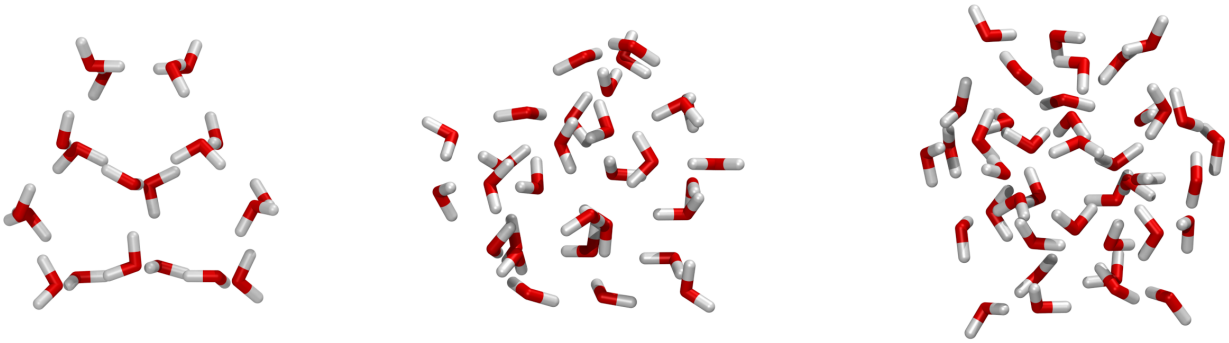

Figure 1: Molecular structures of (a) $(H_2O)_{20}$, (b) $(H_2O)_{30}$, and (c) $(H_2O)_{40}$ taken from the test set of water clusters of increasing size. All structures in this test set correspond to the global minima as obtained in Ref. 77 using the TIP4P force field.

3 Benchmarking the db-MBE for water clusters of increasing size

As our first test case, we consider water clusters of increasing size, consisting of 6 to 55 water molecules. For each cluster size, we employ the global minimum structure determined using the TIP4P force field,[76,77] as available from Ref. 77. As examples, the considered structures of $(H_2O)_{20}$, $(H_2O)_{30}$, and $(H_2O)_{40}$ are shown in Fig. 1. This test set has previously been used extensively by Herbert and co-workers[22,27–29] to assess the accuracy of many-body expansions.

For each cluster size, we have calculated the total interaction energy,

$$E^{\mathrm{MBE}}_{\mathrm{int,\,tot}} = E^{(n)}_{\mathrm{MBE}} - \sum_I E_I, \tag{23}$$

using different MBEs (see below) and compared it to the total interaction energy obtained with the help of a full, supermolecular calculations of the respective water cluster,

$$E^{\mathrm{super}}_{\mathrm{int,\,tot}} = E^{\mathrm{super}}_{\mathrm{tot}} - \sum_I E_I. \tag{24}$$

In Fig. 2, we plot the error in the total interaction energy for different MBEs

$$\Delta E_{\mathrm{int}}^{\mathrm{MBE}} = E_{\mathrm{int,tot}}^{\mathrm{MBE}} - E_{\mathrm{int,tot}}^{\mathrm{super}}. \tag{25}$$

as a function of the cluster size $n = 6, \ldots, 55$. Here, we have performed DFT calculations using the BP86 GGA functional (upper part of Fig. 2) as well as the B3LYP hybrid functional[63–65] (lower part of Fig. 2) in combination with a DZP basis set. The data underlying the plots in Fig. 2 are given in Section S2 of the Supporting Information.

Note that we take the supermolecular calculations for the respective water clusters as our reference, and do not correct for basis-set superposition error, which is only significant for the accuracy of MBEs if large basis sets containing diffuse functions are used.[23,78] Thus, while the total interaction energies might not accurately agree with the results of high-level calculations, our comparison is internally consistent and allows us to assess the error introduced by the truncated MBEs. Generally, the errors observed for low-order MBEs have been found to be size-extensive.[29] Here, we consider an error in the total interaction energy below 1 kcal/mol (or 4.2 kJ/mol) per monomer, corresponding to chemical accuracy for the interaction energy per monomer, as a reasonable target. Of course, this can still result in a substantial error in the total energies for larger clusters, and different accuracy targets (such as "dynamical accuracy" of 0.37 kJ/mol per monomer[79]) might be needed depending on the applications at hand, in particular if larger clusters are considered.

Fig. 2a plots the error in the total interaction energy for the isolated MBEs, i.e., the MBEs have been performed using calculations for the isolated monomers and dimers. For the conventional energy-based two-body expansion [eb-MBE(2), cyan squares] the error increases roughly linearly with the number of fragments. For BP86/DZP (upper panel), it amounts to 10.3 kJ/mol per monomer for $(H_2O)_{10}$ and to 14.0 kJ/mol per monomer for $(H_2O)_{55}$, whereas for B3LYP/DZP the error is 7.9 kJ/mol per monomer for $(H_2O)_{10}$ and 9.9 kJ/mol per monomer for $(H_2O)_{55}$. We note that while our general trend of a roughly linear increase

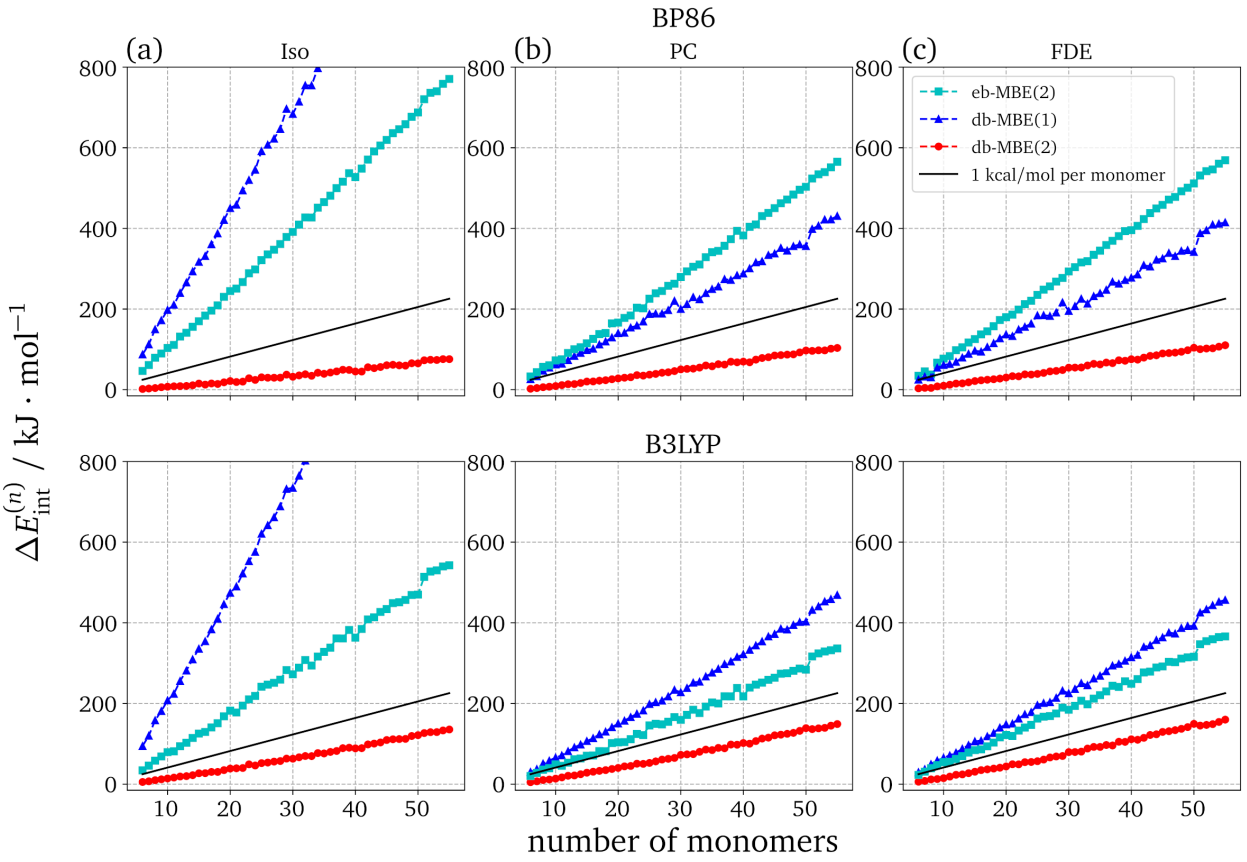

Figure 2: Error in the total interaction energy $\Delta E_{\mathrm{int}}^{(n)}$ for $(H_2O)_N$ clusters of increasing size ($N = 6, \ldots, 55$) for an energy-based two-body expansion [eb-MBE(2), cyan squares] as well as for a density-based many-body expansion of first [db-MBE(1), blue triangles] and second [db-MBE(2), red circles] order. Our target accuracy of 1 kcal/mol per monomer is indicated by the black line. The MBEs have been performed using (a) calculations of the isolated monomers and dimers ("Iso"), (b) using electrostatic point-charge embedding ("PC"), and (c) using a frozen-density embedding potential ("FDE"). All results have been obtained in DFT calculations with the BP86 GGA functional (upper panels) and the B3LYP hybrid functional (lower panels) in combination with a DZP basis set.

agrees with the previous results of Herbert and coworkers,[28] the magnitude of the errors differs. For B3LYP/cc-pVDZ, Ref. 28 reports an average error of only 4.4 kJ/mol per monomer, but the results presented in Ref. 28 also show a strong basis-set dependence.

The errors in the total interaction energy for a density-based MBE of first order [db-MBE(1), blue triangles] and second order [db-MBE(2), red circles] are also included in Fig. 2a. The first-order db-MBE(1), which requires only calculations for the monomers, leads to results that are clearly worse than for the eb-MBE(2), with an error of 25.2 kJ/mol per monomer for $(H_2O)_{55}$ in the BP86/DZP calculations, respectively. However, the second-order db-MBE(2) drastically improves upon the eb-MBE(2), with an error in the total interaction energy per monomer that is well below the threshold of chemical accuracy. For BP86/DZP, the error is 0.7 kJ/mol per monomer for $(H_2O)_{10}$ and 1.4 kJ/mol per monomer for $(H_2O)_{55}$.

Fig. 2b shows the errors in the total interaction energies for the corresponding MBEs performed in the presence of an electrostatic point-charge embedding potential in the calculations of the monomers and dimers. Here, we used the charges provided by the TIP3P water model.[69] First, we note that the inclusion of the point-charge embedding significantly improves the performance of the eb-MBE(2) compared to the isolated MBE, with errors of 7.3 kJ/mol per monomer for $(H_2O)_{10}$ and 10.3 kJ/mol per monomer for $(H_2O)_{55}$ in the BP86/DZP calculations. Also for the first-order db-MBE(1), the errors are significantly reduced and become roughly comparable to those of the eb-MBE(2). For the second-order db-MBE(2), the errors are again drastically reduced and the error per fragment remains below chemical accuracy. For BP86/DZP, it amounts to 0.9 kJ/mol per monomer for $(H_2O)_{10}$ and 1.9 kJ/mol per monomer for $(H_2O)_{55}$. We note that this error is slightly larger than for the isolated db-MBE(2).

Finally, the results for the MBEs using a frozen-density embedding potential in the monomer and dimer calculations are plotted in Fig. 2c. They largely agree with those obtained with point-charge embedding. For BP86/DZP, errors amounts to 7.7 kJ/mol per monomer for $(H_2O)_{10}$ and 10.2 kJ/mol per monomer for $(H_2O)_{55}$ with the eb-MBE(2), com-

pared to 1.0 kJ/mol per monomer for $(H_2O)_{10}$ and 1.9 kJ/mol per monomer for $(H_2O)_{55}$ with the db-MBE(2). This indicates that the use of such a more sophisticated embedding potential does not improve compared to the use of well-chosen point charges. We note that for the eb-MBE(2), Herbert and co-workers found a strong sensitivity on the choice of the embedding charges.[28] Thus, the use of a frozen-density embedding potential might offer an unbiased alternative in cases where no point-charge parametrization is available or where the choice of suitable charges is ambiguous.

Comparing the BP86/DZP (upper panels) and the B3LYP/DZP results (lower panels), we notice that the errors of the eb-MBE are lower in the case of B3LYP. This can be attributed to the strong method dependence of the interaction energies as well as their errors in eb-MBEs for water clusters.[28] For the density-based MBEs, the errors are slightly larger for the B3LYP calculations compared to BP86. This is most likely related to the fact that for hybrid functionals such as B3LYP, the non-additive xc energy contributions have to be approximated using a pure GGA functional, whereas for BP86, the xc energy contributions are handled consistently using the same functional in the db-MBE and in the supermolecular calculation. Results of additional test calculations assessing the influence of the choice of the nonadditive xc functional can be found in Section S1 of the Supporting Information.

Overall, our results for the considered test set of water clusters of increasing size with up to 55 monomers show that a two-body db-MBE(2) outperforms the conventional eb-MBE(2), while requiring the same number of single-point calculations for monomers and dimers. Both for an isolated db-MBE(2) and when using a suitable embedding potential in the db-MBE(2), the error per monomer is well below the threshold of chemical accuracy (1 kcal/mol or 4.2 kJ/mol), even though it does not reach the threshold of dynamical accuracy (0.37 kJ/mol).[79] We further note that already the first-order db-MBE(1), which requires only single-point calculations for the monomers, yields errors that are comparable to those of the eb-MBE(2) if a suitable embedding scheme is used.

4 Benchmarking the db-MBE for isomers of selected water clusters

While the calculations presented in the previous section allow us to judge the absolute error in the total interaction energy, for many applications relative stabilities across a set of similar molecular systems are more relevant, and present another challenging test case for MBEs.[33] Therefore, in this section we assess the ability of MBEs to accurately predict the relative interaction energies of different isomers of water clusters of the same size. We consider the low-energy isomers identified in previous studies for $(H_2O)_6$,[80] $(H_2O)_{16}$,[81] $(H_2O)_{17}$,[81] and $(H_2O)_{20}$.[82] The relative stabilities of the different isomers depend on the structure of the respective hydrogen-bonding networks as well as the strengths of the intermolecular hydrogen bonds. These, in turn, intricately depend on cooperative polarization effects,[15] which are difficult to capture in conventional eb-MBEs.

For our test set, we used the coordinates of the different isomers available in Refs. 80–82 and performed calculations using both the eb-MBE and the db-MBE of increasing order with BP86/DZP, considering both the isolated and point-charge embedded case. Results for the frozen-density embedded MBEs are very close to those obtained with point-charge embedding and are, therefore, not discussed in the following. Similarly, no significantly different observations are made when applying B3LYP/DZP. These additional results can be found in Section S3 of the Supporting Information.

For each cluster size, we consider the total interaction energies of the different isomers, relative to the one of the lowest-energy isomer, i.e.,

$$E_{\mathrm{int,rel}}^{\text{isomer A}} = E_{\mathrm{int,tot}}^{\text{isomer A}} - E_{\mathrm{int,tot}}^{\text{isomer 0}}, \tag{26}$$

where $E_{\mathrm{int,tot}}$ is calculated according to Eq. (23) and where the superscripts "isomer A" and "isomer 0" denote the considered isomer as well as the lowest-energy isomer, respectively.

Table 1: Interaction energies (BP86/DZP, in kJ/mol) of the book, ring, cage, and prism isomers of the water hexamer $(H_2O)_6$ relative to the book isomer as calculated with the energy-based MBE up to forth order [eb-MBE(n), $n = 2, 3, 4$] as well as the density-based MBE up to forth order [db-MBE(n), $n = 1, 2, 3, 4$]. The relative interaction energies from supermolecular calculations are given as reference. Included are results from the isolated MBEs ("iso") as well as embedded MBEs using point charges ("PC").

	isomer	$E_{\text{int,rel}}^{\text{super}}$	$E_{\text{int,rel}}^{\text{eb-MBE}(n)}$			$E_{\text{int,rel}}^{\text{db-MBE}(n)}$			
			$n=2$	$n=3$	$n=4$	$n=1$	$n=2$	$n=3$	$n=4$
iso	Book	0.00	0.00	0.00	0.00	0.00	0.00	0.00	0.00
	Ring	+2.14	+9.22	+7.16	+3.23	+11.34	+3.09	−0.68	+1.47
	Cage	+3.65	−2.33	−1.01	+3.43	−9.61	+4.11	+6.34	+3.46
	Prism	+5.89	−0.05	+1.15	+5.45	−13.69	+6.55	+8.21	+6.18
PC	Book	0.00	0.00	0.00	0.00	0.00	0.00	0.00	0.00
	Ring	+2.14	+3.84	+5.47	+2.87	+5.79	+4.16	+1.56	+2.15
	Cage	+3.65	+1.63	0.00	+3.51	−3.26	+2.79	+4.76	+3.32
	Prism	+5.89	+3.71	+1.68	+5.89	−6.11	+4.80	+7.07	+5.40

Note that this relative interaction energy differs from the commonly considered relative total energy,

$$\begin{aligned} E_{\text{rel}}^{\text{isomer A}} &= E_{\text{tot}}^{\text{isomer A}} - E_{\text{tot}}^{\text{isomer 0}} \\ &= \Big(E_{\text{int,tot}}^{\text{isomer A}} + \sum_I E_I^{\text{isomer A}}\Big) - \Big(E_{\text{int,tot}}^{\text{isomer 0}} + \sum_I E_I^{\text{isomer 0}}\Big) \\ &= E_{\text{int,rel}}^{\text{isomer A}} + \Big(\sum_I E_I^{\text{isomer A}} - \sum_I E_I^{\text{isomer 0}}\Big). \end{aligned} \tag{27}$$

Here, the difference, $\sum_I E_I^{\text{isomer A}} - \sum_I E_I^{\text{isomer 0}}$ is due to differences in the geometries of the water monomers for the two isomers. However, since this term is calculated consistently with all MBEs we do not include it in our comparison, as it might otherwise obscure the relative accuracy of the MBEs.

First, we consider the book, ring, cage, and prism isomers of the water hexamer (cf. Ref. 80). These structures are shown in Fig. 3b. The interaction energies of these $(H_2O)_6$ isomers,

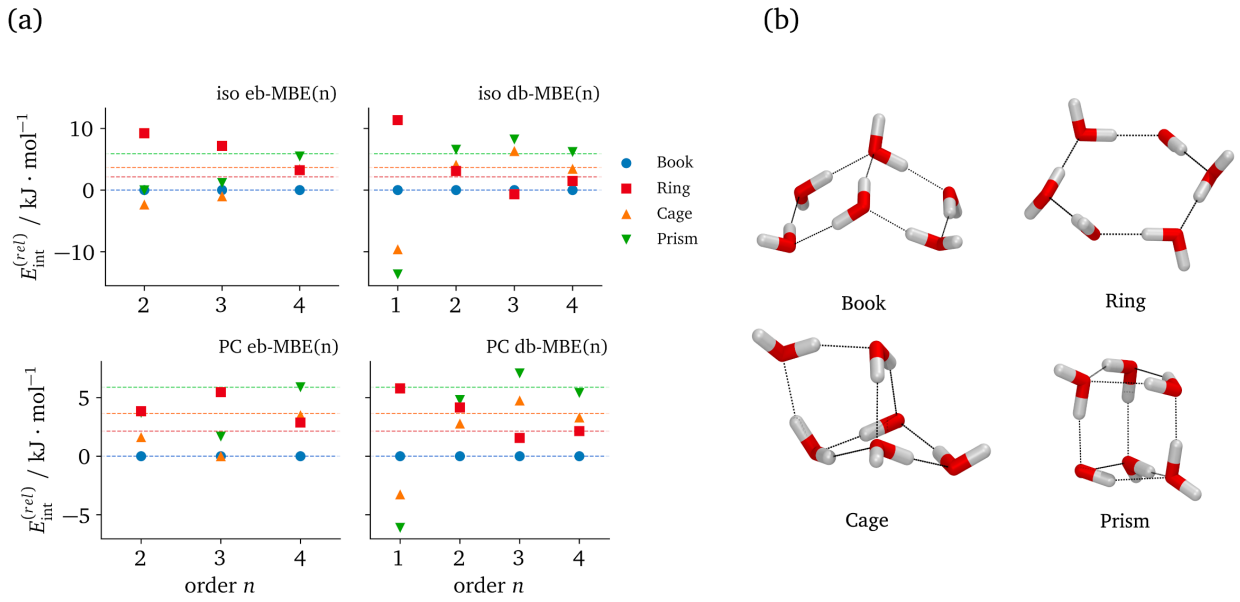

Figure 3: (a) Interaction energies (BP86/DZP) of the book (blue circles), ring (red squares), cage (orange up-triangles), and prism (green down-triangles) isomers of the water hexamer $(H_2O)_6$ relative to the book isomer as calculated with the energy-based MBE [eb-MBE(n), $n = 2, 3, 4$, left panels] as well as the density-based MBE [db-MBE(n), $n = 1, 2, 3, 4$, right panels]. The horizontal dashed lines indicate the corresponding reference values from supermolecular calculations. Included are results from both the isolated MBEs ("iso", upper panels) and the embedded MBEs using point charges ("PC", lower panels). (b) Molecular structures of the book, cage, prism, and ring isomer of the water hexamer.

relative to the book isomer, are given in Table 1 and are visualized in Fig. 3a. In the supermolecular BP86/DZP calculations, the interaction energy is the largest for the book isomer, while the other three considered isomers show slightly smaller interaction energies. The ring isomer has the second largest interaction energy, which is 2.14 kJ/mol smaller than for the book isomer. This is followed by the cage and prism isomers, with interaction energies that are 3.65 kJ/mol and 5.89 kJ/mol smaller than for the book isomer. Reproducing these small differences in interaction energies is challenging for MBEs, in particular as these are not correlated with the number of intermolecular hydrogen bonds. For instance, the ring isomer only exhibits six hydrogen bonds (compared to eight for the cage isomer), but is significantly stabilized by cooperative polarization effects.

The energy-based two- and three-body expansions fail to reproduce the correct order of interaction energies in the isomers, both for the isolated and for point-charge embedded eb-MBE. In all cases, the ring isomer is predicted to have the lowest interaction energy, whereas the interaction energy of the cage isomer is overestimated. Only with the four-body eb-MBEs the correct ordering is reproduced, with errors in the relative interaction energies that are smaller than 1 kJ/mol for all isomers for the embedded eb-MBE(4). These findings for the eb-MBE are in agreement with previous calculations for water hexamers[83] and with the general finding that at least a four-body eb-MBE(4) is necessary to achieve accurate results for water clusters.[23,29]

At first order (i.e., using only monomer calculations), the db-MBE also fails dramatically and the resulting ordering only reflects the number of intermolecular hydrogen bonds. However, already for a two-body db-MBE the results are significantly improved compared to the eb-MBE(2). Both the isolated and the embedded db-MBE(2) correctly identify the book isomer as the one with the largest interaction energy. Moreover, they correctly predict a larger interaction energy for the ring isomer than for the prism isomer and correctly find that despite its larger number of hydrogen bonds, the prism isomer has the smallest interaction energy. The db-MBE(3) further improves upon the two-body expansions. For the isolated

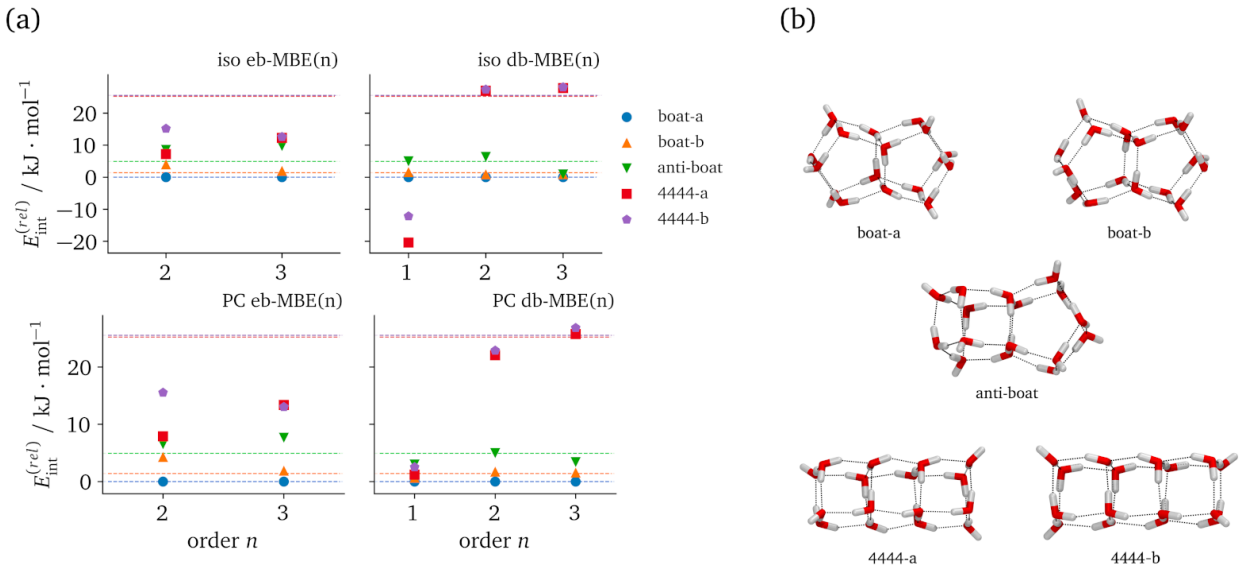

Figure 4: (a) Interaction energies (BP86/DZP) of five isomers of $(H_2O)_{16}$ relative to the boat-a isomer as calculated with the energy-based MBE [eb-MBE(n), $n = 2, 3$, left panels] as well as the density-based MBE [db-MBE(n), $n = 1, 2, 3$, right panels]. The horizontal dashed lines indicate the corresponding reference values from supermolecular calculations. Included are results from both the isolated MBEs ("iso", upper panels) and the embedded MBEs using point charges ("PC", lower panels). (b) Molecular structures of the considered isomer of $(H_2O)_{16}$

db-MBE(3), the ring isomer is over-stabilized, but for the embedded db-MBE(3) the correct ordering of the interaction energies is obtained. Finally, for the embedded db-MBE(4), the errors in the relative interaction energies drop below 0.5 kJ/mol for all four isomers.

As a second test case, we consider the five isomers of $(H_2O)_{16}$ studied in Ref. 81. Previous results for this test set using the eb-MBE can be found in Ref. 84. The interaction energies obtained in supermolecular BP86/DZP calculations as well as the corresponding eb-MBEs and db-MBEs are given in Table 2 and are visualized in Fig. 4, which also shows the molecular structures of the considered isomers. In the supermolecular calculations, the boat-a and boat-b isomers show the largest interaction energies, with a difference of only 1.39 kJ/mol between the two. For the anti-boat isomer, a slightly lower interaction energy is found, which differs by only 4.92 kJ/mol from the one of the boat-a isomer. The 4444-a and 4444-b isomers show almost identical interaction energies (differing by only 0.31 kJ/mol), which are ca. 25 kJ/mol

Table 2: Interaction energies (BP86/DZP, in kJ/mol) of five isomers of $(H_2O)_{16}$ relative to the boat-a isomer as calculated with the energy-based MBE of second and third order [eb-MBE(n), $n = 2, 3$] as well as the density-based MBE of first, second, and third order [db-MBE(n), $n = 1, 2, 3$]. The relative interaction energies from supermolecular calculations are given as reference. Included are results from the isolated MBEs ("iso") as well as embedded MBEs using point charges ("PC").

	isomer	$E_{\text{int,rel}}^{\text{super}}$	$E_{\text{int,rel}}^{\text{eb-MBE}(n)}$		$E_{\text{int,rel}}^{\text{db-MBE}(n)}$		
			$n = 2$	$n = 3$	$n = 1$	$n = 2$	$n = 3$
iso	boat-a	0.00	0.00	0.00	0.00	0.00	0.00
	boat-b	+1.39	+4.05	+1.99	+1.62	+0.91	+0.95
	anti-boat	+4.92	+8.53	+9.74	+4.93	+6.34	+0.86
	4444-a	+25.22	+7.19	+12.26	−20.43	+26.95	+27.81
	4444-b	+25.53	+15.16	+12.60	−12.19	+27.40	+28.09
PC	boat-a	0.00	0.00	0.00	0.00	0.00	0.00
	boat-b	+1.39	+4.30	+1.91	+0.68	+1.74	+1.58
	anti-boat	+4.92	+6.52	+7.65	+2.98	+4.97	+3.39
	4444-a	+25.22	+7.89	+13.37	+1.19	+22.05	+25.76
	4444-b	+25.53	+15.55	+13.02	+2.52	+22.89	+26.85

lower than for the boat-a structure.

The eb-MBE(2) fails to correctly reproduce the relative interaction energies. It largely underestimates the energy splitting between the boat-a and the two 4444 isomers, and finds an interaction energy difference of ca. 8 kJ/mol between the almost isoenergetic 4444-a and 4444-b isomers. This energy difference found in the eb-MBE(2) calculations reflects the differences in the electrostatic interaction between the dipole moments of the water molecules. While in the 4444-a isomer, the four stacked tetramers are aligned in an electrostatically favorable antiparallel fashion (*abab*), they are arranged in an *aabb* configuration with a parallel alignment of the dipoles between the first and second as well as the third and fourth layer.

Going to the eb-MBE(3) significantly improves by yielding the correct ordering, but still fails to reproduce the interaction energy differences between the isomers accurately. While the energy difference between the boat-a and boat-b isomers is accurate to within 0.6 kJ/mol for both the isolated and the embedded eb-MBE(3), the relative interaction energy of the anti-boat isomer is too low by 4.83 kJ/mol and 2.73 kJ/mol for the isolated and the embedded expansion, respectively. The interaction energy splitting between the 4444-a and the 4444-b isomer is now smaller than 0.35 kJ/mol. Both isomers are overstabilized compared to the boat isomers, with a relative interaction energy that is about half as large as in the supermolecular calculation. This failure of the eb-MBE to accurately reproduce the relative energies of the considered $(H_2O)_{16}$ isomers is in agreement with the previous studies.[84]

In contrast, already the two-body db-MBE(2) correctly reproduces both the ordering of the interaction energies for the different isomers and the relative interaction energies themselves, including for the splitting between the 4444-a and 4444-b isomers. The maximum error of the relative interaction energies amounts to 1.9 kJ/mol and 2.64 kJ/mol for the isolated and for the point-charge embedded db-MBE(2), respectively. While compared to the isolated db-MBE(2) the embedded db-MBE(2) improves for the low-lying boat and anti-boat isomers, it overestimates the interaction energies of the 4444-a and 4444-b isomers.

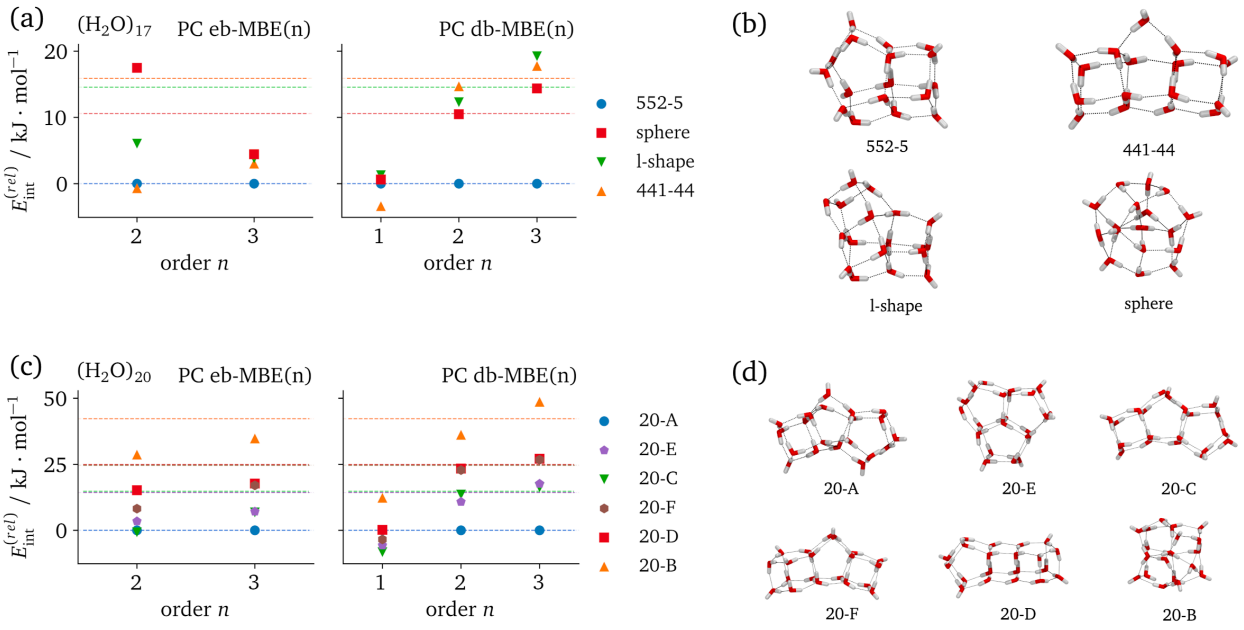

Figure 5: (a,c) Interaction energies (BP86/DZP) of isomers of (a) $(H_2O)_{17}$ and (c) $(H_2O)_{20}$ relative to the respective lowest-energy isomer, as calculated with the energy-based MBE [eb-MBE(n), $n = 2, 3$, left panels] as well as the density-based MBE [db-MBE(n), $n = 1, 2, 3$, right panels] using point-charge embedding. The horizontal dashed lines indicate the corresponding reference values from supermolecular calculations. (b,d) Molecular structures of the considered isomer of (b) $(H_2O)_{17}$ and (d) $(H_2O)_{20}$.

When going to the three-body db-MBE(3), the accuracy further improves, and for the case of the embedded db-MBE(3), the maximum error in the relative interaction energies amounts to only 1.32 kJ/mol.

As our third test case, we chose the four isomers of $(H_2O)_{17}$ investigated in Ref. 81 (see Fig. 5b). Our results for the point-charge embedded eb-MBE and db-MBE are given in Table 3 and are shown in Fig. 5a. The results for the isolated MBEs can be found in the Supporting Information. In our BP86/DZP supermolecular calculations, the 552-5 isomer is the one with the largest interaction energy, followed by the sphere isomer with an interaction energy that is smaller by 10.57 kJ/mol, and the l-shape and 441-44 isomers that are 14.56 kJ/mol and 15.89 kJ/mol, respectively, above the most stable one.

The two-body as well as three-body eb-MBEs dramatically fail to reproduce both the

Table 3: Interaction energies (BP86/DZP, in kJ/mol) of isomers of $(H_2O)_{17}$ and $(H_2O)_{20}$ relative to the respective lowest-energy isomer, as calculated with the energy-based MBE of second and third order [eb-MBE(n), $n = 2, 3$] as well as the density-based MBE of first, second, and third order [db-MBE(n), $n = 1, 2, 3$] using point-charge embedding.

	isomer	$E_{\text{int,rel}}^{\text{super}}$	$E_{\text{int,rel}}^{\text{eb-MBE}(n)}$		$E_{\text{int,rel}}^{\text{db-MBE}(n)}$		
			$n = 2$	$n = 3$	$n = 1$	$n = 2$	$n = 3$
$(H_2O)_{17}$	552-5	0.00	0.00	0.00	0.00	0.00	0.00
	sphere	+10.57	+17.48	+4.44	+0.63	+10.48	+14.38
	l-shape	+14.56	+6.03	+3.79	+1.29	+12.30	+19.23
	441-44	+15.89	−0.68	+3.03	−3.38	+14.70	+17.77
$(H_2O)_{20}$	20-A	0.00	0.00	0.00	0.00	0.00	0.00
	20-E	+14.27	+3.42	+7.11	−5.68	+10.81	+17.65
	20-C	+14.79	−0.75	+6.75	−8.30	+13.55	+16.25
	20-F	+24.63	+8.17	+17.02	−3.48	+22.80	+26.71
	20-D	+24.96	+15.15	+17.70	+0.14	+23.38	+27.08
	20-B	+42.23	+28.68	+34.79	+12.34	+36.19	+48.69

ordering and the energy differences between all pairs of isomers. In contrast, the db-MBE(2) and db-MBE(3) show a substantial improvement compared to the eb-MBE. For the two-body db-MBE(2), the ordering of the four isomers is reproduced correctly, with the relative interaction energies of the l-shape and 441-44 isomers overestimated by 2.26 kJ/mol and 1.19 kJ/mol, respectively. For the three-body db-MBE(3), the overall accuracy becomes slightly worse. Now, the 552-5 isomer is overstabilized compared to the other three isomers and the order of the l-shape and 441-44 isomers is reversed, while at the same time the interaction energy difference between the sphere isomer and the l-shape and 441-44 isomers becomes more accurate.

Finally, we consider the six low-energy isomers of $(H_2O)_{20}$, which have been identified and optimized by Gadre and coworkers.[82] Following Ref. 82, we label these isomers 20-A to 20-F (see Fig. 5d). The corresponding results are included in Table 3 and are visualized in Fig. 5c. With supermolecular BP86/DZP calculations, 20-A has the largest interaction

energy. The pairs 20-E and 20-C as well as 20-F and 20-D are almost isoenergetic, with an interaction energy of ca. 14.5 kJ/mol and ca. 24.8 kJ/mol, respectively, lower than for 20-A. While again, the two-body eb-MBE(2) fails to correctly reproduce this correct ordering of the isomers, the three-body eb-MBE(3) yields the correct pattern, even though the order is reversed for the pair 20-C and 20-E. However, the magnitude of the interaction energy differences is severely underestimated also with the eb-MBE(3).

In contrast, the db-MBE(2) yields the correct ordering for all six isomers and significantly improves for the interaction energy differences compared to the eb-MBE(3). Still, the relative interaction energies are too low for all isomers by up to 6 kJ/mol, and the splitting between 20-E and 20-C is too large by 2.22 kJ/mol. With the db-MBE(3), the overall picture is slightly improved, even though all relative interaction energies are now overestimated by up to 6.5 kJ/mol.

Overall, for interaction energy differences between different isomers of water clusters $(H_2O)_n$ with $n = 6, 16, 17, 20$ we find that in general, the eb-MBE is not able to correctly reproduce the interaction energy differences between the different isomers as obtained from a supermolecular calculation. Mostly, even the ordering of the considered isomers is not described correctly. This even holds if a point-charge embedded eb-MBE is employed. Our findings for the eb-MBE are in agreement with previous results that demonstrated the need for including four-body or even higher-order contributions for challenging systems such as water clusters (see, e.g., Ref. 29 and references therein). These shortcomings of the eb-MBE are rectified already by the two-body db-MBE(2), which generally accurately reproduces both the energy ordering of the considered isomers as well as the interaction energy differences. Overall, the results obtained with the db-MBE(3) are comparable in accuracy to those from the db-MBE(2), and show not clear improvement in most cases.

Across our test set, we find a mean unsigned error in the relative interaction energies of 0.13 kJ/mol per fragment and of 0.14 kJ/mol per fragment for the db-MBE(2) and db-MBE(3), respectively. The maximum errors amount to 0.34 kJ/mol per fragment and of

0.32 kJ/mol per fragment for the db-MBE(2) and db-MBE(3), respectively, and are thus below the threshold of dynamical accuracy.[79]

5 Conclusions and Outlook

Conventionally, the many-body expansion is performed based on the total energies of monomer, dimer, trimer etc. fragments, but this energy-based MBE suffers from a slow convergence with the expansion order. For systems such as water clusters, that show strong polarization and other cooperative effects, it has been previously demonstrated that the inclusion of three- and four-body contributions is mandatory to reach a sufficient accuracy.[23,27,28] This still holds if the eb-MBE is combined with suitable embedding schemes for the fragment calculations.

To alleviate this shortcoming, the MBE can be performed for the electron density, which provides a density-based energy correction that accounts for many-body polarization effects already at low expansion orders.[34] In fact, with an exact embedding scheme (e.g., with frozen-density embedding in combination with an exact treatment of the nonadditive kinetic energy[85,86]), the correct total electron density could in principle already be reproduced at the one-body level, i.e., as the sum of (embedded) monomer densities. While even in this case, the eb-MBE fails to reproduce the supermolecular total energy, the db-MBE becomes exact if the MBE of the electron density agrees with the supermolecular electron density, assuming that exact nonadditive density functional are used.

From a more practical point of view, the db-MBE can be considered as an ONIOM-style hybrid scheme, in which an eb-MBE is used as the high-level method, whereas an orbital-free DFT treatment is used as the low-level method. This is similar to hybrid schemes such as the hybrid-many body interactions (HMBI) method of Beran and coworkers,[11,36] which uses a polarizable force field as low-level method. Here, the db-MBE offers the advantage that it treats the many-body polarization effect fully quantum-chemically and does not rely on any

parametrization.

In the present study, we have assessed the accuracy of the db-MBE for test sets of water clusters. For water clusters of increasing size, we could show that already at second order (i.e., for a two-body expansion) the db-MBE yields errors that are below the threshold of chemical accuracy for the interaction energy per fragment. For the considered isomers of water clusters, the second-order db-MBE(2) is able to accurately predict the energetic ordering of as well as the energy differences between the different isomers.

While already an isolated db-MBE drastically improves compared to an eb-MBE, we find that in general the use of a suitable embedding scheme in the fragment calculations further improves the accuracy of the db-MBE. Here, we found that for water clusters a point-charge embedding is generally sufficient and that the use of a frozen-density embedding potential does not yield further improvements.

We note that the db-MBE does not require any additional quantum-chemical calculations compared to an eb-MBE of the same order. The evaluation of the density-based energy correction only requires the calculation of the electron densities and electrostatic potentials of all fragments on a suitable numerical integration grid. This step adds some computational overhead, but does not alter the overall scaling of the MBE.

In the present study, we have only considered MBEs based on DFT calculations, which allow for a consistent comparison to supermolecular results. However, the formalism of the db-MBE is not restricted to DFT. The calculation of the density-based interaction energy correction $E^{(n)}_{\text{db-corr}}$ only requires the fragments' electron densities and their associated Coulomb potentials, and it can thus be calculated using any quantum-chemical method that is able to provide an electron density. We will explore the combination of the db-MBE with the use of accurate wave-function based quantum-chemical methods in our future work.

Acknowledgement

Funding from the Deutsche Forschungsgemeinschaft for the development of PyADF (Project Suresoft, JA 2329/7-1) is gratefully acknowledged.

References

(1) Gordon, M. S.; Fedorov, D. G.; Pruitt, S. R.; Slipchenko, L. V. Fragmentation Methods: A Route to Accurate Calculations on Large Systems. *Chem. Rev.* **2012**, *112*, 632–672.

(2) Pruitt, S. R.; Bertoni, C.; Brorsen, K. R.; Gordon, M. S. Efficient and Accurate Fragmentation Methods. *Acc. Chem. Res.* **2014**, *47*, 2786–2794.

(3) Raghavachari, K.; Saha, A. Accurate Composite and Fragment-Based Quantum Chemical Models for Large Molecules. *Chem. Rev.* **2015**, *115*, 5643–5677.

(4) Collins, M. A.; Bettens, R. P. A. Energy-Based Molecular Fragmentation Methods. *Chem. Rev.* **2015**, *115*, 5607–5642.

(5) Gordon, M. S., Ed. *Fragmentation: Toward Accurate Calculations on Complex Molecular Systems*, 1st ed.; Wiley: Hoboken, NJ, 2017.

(6) Fedorov, D. G. The fragment molecular orbital method: theoretical development, implementation in GAMESS, and applications. *WIREs Comput. Mol. Sci.* **2017**, *7*, e1322.

(7) Fedorov, D. G.; Olson, R. M.; Kitaura, K.; Gordon, M. S.; Koseki, S. A new hierarchical parallelization scheme: Generalized distributed data interface (GDDI), and an application to the fragment molecular orbital method (FMO). *J. Comput. Chem.* **2004**, *25*, 872–880.

(8) Fletcher, G. D.; Fedorov, D. G.; Pruitt, S. R.; Windus, T. L.; Gordon, M. S. Large-Scale MP2 Calculations on the Blue Gene Architecture Using the Fragment Molecular Orbital Method. *J. Chem. Theory Comput.* **2012**, *8*, 75–79.

(9) Findlater, A. D.; Zahariev, F.; Gordon, M. S. Combined Fragment Molecular Orbital Cluster in Molecule Approach to Massively Parallel Electron Correlation Calculations for Large Systems. *J. Phys. Chem. A* **2015**, *119*, 3587–3593.

(10) König, C.; Christiansen, O. Linear-scaling generation of potential energy surfaces using a double incremental expansion. *J. Chem. Phys.* **2016**, *145*, 064105.

(11) Beran, G. J. O.; Nanda, K. Predicting Organic Crystal Lattice Energies with Chemical Accuracy. *J. Phys. Chem. Lett.* **2010**, *1*, 3480–3487.

(12) Yang, J.; Hu, W.; Usvyat, D.; Matthews, D.; Schütz, M.; Chan, G. K.-L. Ab initio determination of the crystalline benzene lattice energy to sub-kilojoule/mole accuracy. *Science* **2014**, *345*, 640–643.

(13) Gadre, S. R.; Yeole, S. D.; Sahu, N. Quantum Chemical Investigations on Molecular Clusters. *Chem. Rev.* **2014**, *114*, 12132–12173.

(14) Beran, G. J. O. Modeling Polymorphic Molecular Crystals with Electronic Structure Theory. *Chem. Rev.* **2016**, *116*, 5567–5613.

(15) Xantheas, S. S. Cooperativity and hydrogen bonding network in water clusters. *Chem. Phys.* **2000**, *258*, 225–231.

(16) Cisneros, G. A.; Wikfeldt, K. T.; Ojamäe, L.; Lu, J.; Xu, Y.; Torabifard, H.; Bartók, A. P.; Csányi, G.; Molinero, V.; Paesani, F. Modeling Molecular Interactions in Water: From Pairwise to Many-Body Potential Energy Functions. *Chem. Rev.* **2016**, *116*, 7501–7528.

(17) Pham, C. H.; Reddy, S. K.; Chen, K.; Knight, C.; Paesani, F. Many-Body Interactions in Ice. *J. Chem. Theory Comput.* **2017**, *13*, 1778–1784.

(18) Stoll, H.; Preuß, H. On the direct calculation of localized HF orbitals in molecule clusters, layers and solids. *Theor. Chim. Acta* **1977**, *46*, 11–21.

(19) Kaplan, I. G. *Theory of molecular interactions*; Elsevier: Amsterdam, 1986.

(20) Rościszewski, K.; Paulus, B.; Fulde, P.; Stoll, H. Ab initio calculation of ground-state properties of rare-gas crystals. *Phys. Rev. B* **1999**, *60*, 7905–7910.

(21) Cui, J.; Liu, H.; Jordan, K. D. Theoretical Characterization of the (H2O)21 Cluster: Application of an n-body Decomposition Procedure. *J. Phys. Chem. B* **2006**, *110*, 18872–18878.

(22) Richard, R. M.; Lao, K. U.; Herbert, J. M. Understanding the many-body expansion for large systems. I. Precision considerations. *J. Chem. Phys.* **2014**, *141*, 014108.

(23) Liu, K.-Y.; Herbert, J. M. Understanding the many-body expansion for large systems. III. Critical role of four-body terms, counterpoise corrections, and cutoffs. *J. Chem. Phys.* **2017**, *147*, 161729.

(24) Dahlke, E. E.; Truhlar, D. G. Electrostatically Embedded Many-Body Expansion for Large Systems, with Applications to Water Clusters. *J. Chem. Theory Comput.* **2007**, *3*, 46–53.

(25) Liu, J.; Qi, L.-W.; Zhang, J. Z. H.; He, X. Fragment Quantum Mechanical Method for Large-Sized Ion–Water Clusters. *J. Chem. Theory Comput.* **2017**, *13*, 2021–2034.

(26) Liu, K.-Y.; Herbert, J. M. Energy-Screened Many-Body Expansion: A Practical Yet Accurate Fragmentation Method for Quantum Chemistry. *J. Chem. Theory Comput.* **2020**, *16*, 475–487.

(27) Richard, R. M.; Lao, K. U.; Herbert, J. M. Aiming for Benchmark Accuracy with the Many-Body Expansion. *Acc. Chem. Res.* **2014**, *47*, 2828–2836.

(28) Lao, K. U.; Liu, K.-Y.; Richard, R. M.; Herbert, J. M. Understanding the many-body expansion for large systems. II. Accuracy considerations. *J. Chem. Phys.* **2016**, *144*, 164105.

(29) Herbert, J. M. Fantasy versus reality in fragment-based quantum chemistry. *J. Chem. Phys.* **2019**, *151*, 170901.

(30) Dahlke, E. E.; Truhlar, D. G. Electrostatically Embedded Many-Body Expansion for Simulations. *J. Chem. Theory Comput.* **2008**, *4*, 1–6.

(31) Bygrave, P. J.; Allan, N. L.; Manby, F. R. The embedded many-body expansion for energetics of molecular crystals. *J. Chem. Phys.* **2012**, *137*, 164102.

(32) Wen, S.; Beran, G. J. O. Accurate Molecular Crystal Lattice Energies from a Fragment QM/MM Approach with On-the-Fly Ab Initio Force Field Parametrization. *J. Chem. Theory Comput.* **2011**, *7*, 3733–3742.

(33) Veccham, S. P.; Lee, J.; Head-Gordon, M. Making many-body interactions nearly pairwise additive: The polarized many-body expansion approach. *J. Chem. Phys.* **2019**, *151*, 194101.

(34) Schmitt-Monreal, D.; Jacob, Ch. R. Frozen-density embedding-based many-body expansions. *Int. J. Quantum Chem.* **2020**, *120*, e26228.

(35) Tschumper, G. S. Multicentered integrated QM:QM methods for weakly bound clusters: An efficient and accurate 2-body:many-body treatment of hydrogen bonding and van der Waals interactions. *Chem. Phys. Lett.* **2006**, *427*, 185–191.

(36) Beran, G. J. O. Approximating quantum many-body intermolecular interactions in molecular clusters using classical polarizable force fields. *J. Chem. Phys.* **2009**, *130*, 164115.

(37) Mayhall, N. J.; Raghavachari, K. Molecules-in-Molecules: An Extrapolated Fragment-Based Approach for Accurate Calculations on Large Molecules and Materials. *J. Chem. Theory Comput.* **2011**, *7*, 1336–1343.

(38) Richard, R. M.; Herbert, J. M. A generalized many-body expansion and a unified view of fragment-based methods in electronic structure theory. *J. Chem. Phys.* **2012**, *137*, 064113.

(39) Mayhall, N. J.; Raghavachari, K. Many-Overlapping-Body (MOB) Expansion: A Generalized Many Body Expansion for Nondisjoint Monomers in Molecular Fragmentation Calculations of Covalent Molecules. *J. Chem. Theory Comput.* **2012**, *8*, 2669–2675.

(40) Richard, R. M.; Herbert, J. M. Many-Body Expansion with Overlapping Fragments: Analysis of Two Approaches. *J. Chem. Theory Comput.* **2013**, *9*, 1408–1416.

(41) He, X.; Zhang, J. Z. H. The generalized molecular fractionation with conjugate caps/molecular mechanics method for direct calculation of protein energy. *J. Chem. Phys.* **2006**, *124*, 184703.

(42) He, X.; Zhu, T.; Wang, X.; Liu, J.; Zhang, J. Z. H. Fragment Quantum Mechanical Calculation of Proteins and Its Applications. *Acc. Chem. Res.* **2014**, *47*, 2748–2757.

(43) Li, S.; Li, W.; Ma, J. Generalized Energy-Based Fragmentation Approach and Its Applications to Macromolecules and Molecular Aggregates. *Acc. Chem. Res.* **2014**, *47*, 2712–2720.

(44) Gadre, S. R.; Shirsat, R. N.; Limaye, A. C. Molecular Tailoring Approach for Simulation of Electrostatic Properties. *J. Phys. Chem.* **1994**, *98*, 9165–9169.

(45) Babu, K.; Gadre, S. R. Ab initio quality one-electron properties of large molecules: Development and testing of molecular tailoring approach. *J. Comput. Chem.* **2003**, *24*, 484–495.

(46) Sahu, N.; Gadre, S. R. Molecular Tailoring Approach: A Route for ab Initio Treatment of Large Clusters. *Acc. Chem. Res.* **2014**, *47*, 2739–2747.

(47) Harris, J. Simplified method for calculating the energy of weakly interacting fragments. *Phys. Rev. B* **1985**, *31*, 1770–1779.

(48) Averill, F. W.; Painter, G. S. Harris functional and related methods for calculating total energies in density-functional theory. *Phys. Rev. B* **1990**, *41*, 10344–10353.

(49) Cortona, P. Self-consistently determined properties of solids without band-structure calculations. *Phys. Rev. B* **1991**, *44*, 8454–8458.

(50) Jacob, Ch. R.; Neugebauer, J. Subsystem density-functional theory. *WIREs Comput. Mol. Sci.* **2014**, *4*, 325–362.

(51) Kaplan, I. G.; Santamaria, R.; Novaro, O. Non-additive forces in atomic clusters. *Mol. Phys.* **1995**, *84*, 105–114.

(52) Wesolowski, T. A.; Warshel, A. Frozen Density Functional Approach for ab Initio Calculations of Solvated Molecules. *J. Phys. Chem.* **1993**, *97*, 8050–8053.

(53) Humbel, S.; Sieber, S.; Morokuma, K. The IMOMO method: Integration of different levels of molecular orbital approximations for geometry optimization of large systems: Test for n-butane conformation and SN_2 reaction: RCl+Cl^-. *J. Chem. Phys.* **1996**, *105*, 1959–1967.

(54) Chung, L. W.; Sameera, W. M. C.; Ramozzi, R.; Page, A. J.; Hatanaka, M.; Petrova, G. P.; Harris, T. V.; Li, X.; Ke, Z.; Liu, F.; Li, H.-B.; Ding, L.; Morokuma, K. The ONIOM Method and Its Applications. *Chem. Rev.* **2015**, *115*, 5678–5796.

(55) Wesolowski, T. A.; Chermette, H.; Weber, J. Accuracy of approximate kinetic energy functionals in the model of Kohn-Sham equations with constrained electron density: The FH—NCH complex as a test case. *J. Chem. Phys.* **1996**, *105*, 9182–9190.

(56) Wesolowski, T. A. Density functional theory with approximate kinetic energy functionals applied to hydrogen bonds. *J. Chem. Phys.* **1997**, *106*, 8516–8526.

(57) Gomes, A. S. P.; Jacob, Ch. R. Quantum-chemical embedding methods for treating local electronic excitations in complex chemical systems. *Annu. Rep. Prog. Chem., Sect. C* **2012**, *108*, 222.

(58) te Velde, G.; Bickelhaupt, F. M.; Baerends, E. J.; Fonseca Guerra, C.; van Gisbergen, S. J. A.; Snijders, J. G.; Ziegler, T. Chemistry with ADF. *J. Comput. Chem.* **2001**, *22*, 931–967.

(59) Software for Chemistry and Materials, Amsterdam, ADF, Amsterdam density functional program. 2019; URL: http://www.scm.com.

(60) Jacob, Ch. R.; Beyhan, S. M.; Bulo, R. E.; Gomes, A. S. P.; Götz, A. W.; Kiewisch, K.; Sikkema, J.; Visscher, L. PyADF — A scripting framework for multiscale quantum chemistry. *J. Comput. Chem.* **2011**, *32*, 2328–2338.

(61) Becke, A. D. Density-functional exchange-energy approximation with correct asymptotic behavior. *Phys. Rev. A* **1988**, *38*, 3098–3100.

(62) Perdew, J. P. Density-functional approximation for the correlation energy of the inhomogeneous electron gas. *Phys. Rev. B* **1986**, *33*, 8822–8824.

(63) Becke, A. D. Density-functional thermochemistry. III. The role of exact exchange. *J. Chem. Phys.* **1993**, *98*, 5648–5652.

(64) Lee, C.; Yang, W.; Parr, R. G. Development of the Colle-Salvetti correlation-energy formula into a functional of the electron density. *Phys. Rev. B* **1988**, *37*, 785–789.

(65) Stephens, P. J.; Devlin, F. J.; Chabalowski, C. F.; Frisch, M. J. Ab Initio Calculation of Vibrational Absorption and Circular Dichroism Spectra Using Density Functional Force Fields. *J. Phys. Chem.* **1994**, *98*, 11623–11627.

(66) Van Lenthe, E.; Baerends, E. J. Optimized Slater-type basis sets for the elements 1-118. *J. Comput. Chem.* **2003**, *24*, 1142–1156.

(67) Franchini, M.; Philipsen, P. H. T.; Visscher, L. The Becke Fuzzy Cells Integration Scheme in the Amsterdam Density Functional Program Suite. *J. Comput. Chem.* **2013**, *34*, 1819–1827.

(68) Götz, A. W.; Beyhan, S. M.; Visscher, L. Performance of Kinetic Energy Functionals for Interaction Energies in a Subsystem Formulation of Density Functional Theory. *J. Chem. Theory Comput.* **2009**, *5*, 3161–3174.

(69) Jorgensen, W. L.; Chandrasekhar, J.; Madura, J. D.; Impey, R. W.; Klein, M. L. Comparison of simple potential functions for simulating liquid water. *J. Chem. Phys.* **1983**, *79*, 926–935.

(70) Jacob, Ch. R.; Neugebauer, J.; Visscher, L. A flexible implementation of frozen-density embedding for use in multilevel simulations. *J. Comput. Chem.* **2008**, *29*, 1011–1018.

(71) Lembarki, A.; Chermette, H. Obtaining a gradient-corrected kinetic-energy functional from the Perdew-Wang exchange functional. *Phys. Rev. A* **1994**, *50*, 5328–5331.

(72) Neugebauer, J.; Jacob, Ch. R.; Wesolowski, T. A.; Baerends, E. J. An Explicit Quantum Chemical Method for Modeling Large Solvation Shells Applied to Aminocoumarin C151. *J. Phys. Chem. A* **2005**, *109*, 7805–7814.

(73) Ekström, U.; Visscher, L.; Bast, R.; Thorvaldsen, A. J.; Ruud, K. Arbitrary-Order Density Functional Response Theory from Automatic Differentiation. *J. Chem. Theory Comput.* **2010**, *6*, 1971–1980.

(74) Ekström, U.; Bast, R.; Di Remigio, R.; Jacob, Ch. R.; Reine, S.; Juselius, J.; Rebolini, E.; Gomes, A. S. P.; Jensen, S. R.; Reimann, S.; Borgoo, A.; Friese, D. H.; Frediani, L.; Iliaš, M.; Victorovich, Y.; Furness, J. XCFun: Exchange-Correlation functionals with arbitrary order derivatives, Version 2.2.1. 2020; DOI: 10.5281/zenodo.4269992, URL: https://github.com/dftlibs/xcfun/tree/v2.1.1.

(75) Jacob, Ch. R.; Bergmann, T.; Beyhan, S. M.; Brüggemann, J.; Bulo, R. E.; Dresselhaus, T.; Gomes, A. S. P.; Goetz, A. W.; Handzlik, M.; Kiewisch, K.; Klammler, M.; Ridder, L.; Sikkema, J.; Visscher, L.; Wolter, M. PyADF Version 0.98. 2021; DOI: 10.5281/zenodo.4609001, URL: https://github.com/chjacob-tubs/pyadf-releases/tree/v0.98.

(76) Kazachenko, S.; Thakkar, A. J. Improved minima-hopping. TIP4P water clusters, (H2O)n with n?37. *Chem. Phys. Lett.* **2009**, *476*, 120–124.

(77) Kazachenko, S.; Thakkar, A. J. Water nanodroplets: Predictions of five model potentials. *J. Chem. Phys.* **2013**, *138*, 194302.

(78) Ouyang, J. F.; Bettens, R. P. A. When are Many-Body Effects Significant? *J. Chem. Theory Comput.* **2016**, *12*, 5860–5867.

(79) Ouyang, J. F.; Bettens, R. P. A. Many-Body Basis Set Superposition Effect. *J. Chem. Theory Comput.* **2015**, *11*, 5132–5143.

(80) Howard, J. C.; Tschumper, G. S. Benchmark Structures and Harmonic Vibrational Frequencies Near the CCSD(T) Complete Basis Set Limit for Small Water Clusters: (H2O)n = 2, 3, 4, 5, 6. *J. Chem. Theory Comput.* **2015**, *11*, 2126–2136.

(81) Yoo, S.; Aprà, E.; Zeng, X. C.; Xantheas, S. S. High-Level Ab Initio Electronic Structure Calculations of Water Clusters (H2O)16 and (H2O)17: A New Global Minimum for (H2O)16. *J. Phys. Chem. Lett.* **2010**, *1*, 3122–3127.

(82) Furtado, J. P.; Rahalkar, A. P.; Shanker, S.; Bandyopadhyay, P.; Gadre, S. R. Facilitating Minima Search for Large Water Clusters at the MP2 Level via Molecular Tailoring. *J. Phys. Chem. Lett.* **2012**, *3*, 2253–2258.

(83) Dahlke, E. E.; Leverentz, H. R.; Truhlar, D. G. Evaluation of the Electrostatically Embedded Many-Body Expansion and the Electrostatically Embedded Many-Body Ex-

pansion of the Correlation Energy by Application to Low-Lying Water Hexamers. *J. Chem. Theory Comput.* **2008**, *4*, 33–41.

(84) Qi, H. W.; Leverentz, H. R.; Truhlar, D. G. Water 16-mers and Hexamers: Assessment of the Three-Body and Electrostatically Embedded Many-Body Approximations of the Correlation Energy or the Nonlocal Energy As Ways to Include Cooperative Effects. *J. Phys. Chem. A* **2013**, *117*, 4486–4499.

(85) Fux, S.; Jacob, Ch. R.; Neugebauer, J.; Visscher, L.; Reiher, M. Accurate frozen-density embedding potentials as a first step towards a subsystem description of covalent bonds. *J. Chem. Phys.* **2010**, *132*, 164101.

(86) Unsleber, J. P.; Neugebauer, J.; Jacob, Ch. R. No need for external orthogonality in subsystem density-functional theory. *Phys. Chem. Chem. Phys.* **2016**, *18*, 21001–21009.